

Electron acceleration with improved Stochastic Differential Equation method: cutoff shape of electron distribution in test-particle limit

Ryo Yamazaki^a, Tatsuo Yoshida^b, Yuka Tsuchihashi^a, Ryosuke Nakajima^a, Yutaka Ohira^a, Shohei Yanagita^b

^a *Department of Physics and Mathematics, Aoyama Gakuin University, 5-10-1, Fuchinobe, Sagamihara 252-5258, Japan*

^b *College of Science, Ibaraki University, 2-1-1, Bunkyo, Mito 310-8512, Japan*

Abstract

We develop a method of stochastic differential equation to simulate electron acceleration at astrophysical shocks. Our method is based on Itô's stochastic differential equations coupled with a particle splitting, employing a skew Brownian motion where an asymmetric shock crossing probability is considered. Using this code, we perform simulations of electron acceleration at stationary plane parallel shock with various parameter sets, and studied how the cutoff shape, which is characterized by cutoff shape parameter a , changes with the momentum dependence of the diffusion coefficient β . In the age-limited cases, we reproduce previous results of other authors, $a \approx 2\beta$. In the cooling-limited cases, the analytical expectation $a \approx \beta + 1$ is roughly reproduced although we recognize deviations to some extent. In the case of escape-limited acceleration, numerical result fits analytical stationary solution well, but deviates from the previous asymptotic analytical formula $a \approx \beta$.

Keywords: cosmic-ray acceleration, numerical simulation

1. Introduction

Mechanism of particle acceleration is still unknown. Diffusive shock acceleration (Krymskii, 1977; Bell, 1978; Blandford & Ostriker, 1978) is the most plausible if strong shock waves exist as in young supernova remnants (SNRs). We have not yet well constrained model parameters, namely magnetic field strength and degree of magnetohydrodynamic turbulence, although there are observational claims of turbulent, amplified field in young SNRs (Vink & Laming, 2003; Bamba et al., 2003, 2005a,b; Yamazaki et al., 2004; Uchiyama et al., 2007). These are important to estimate maximum attainable energy of both electrons and nuclei (e.g., Yoshida & Yanagita, 1997). Yamazaki et al. (2013) proposed that cutoff shape of electron spectrum around the maximum energy E_{\max} may provide us important information on the cosmic-ray acceleration at young SNRs. They related the cutoff shape parameter a , which is defined by $N(E) \propto \exp[-(E/E_{\max})^a]$, to the energy dependence of the electron diffusion coefficient β (that is, $K \propto E^\beta$) in each case where the maximum electron energy is determined by SNR age, synchrotron cooling and escape from the shock. They found that if the power-law index of the electron spectrum is independently determined by other observations, then the cutoff shape parameter can be constrained by near future hard X-ray observations such as Nuclear Spectroscopic Telescope Array (NuSTAR) (Hailey et al., 2010; Harrison et al., 2013) and ASTRO-H (Takahashi et al., 2010) and/or CTA (Actis et al., 2011). These X-ray and gamma-ray observations will be important for the estimate of β as well as E_{\max} and the magnetic

field strength.

In analysis of Yamazaki et al. (2013), they assumed relations between a and β as $a = 2\beta$, $\beta + 1$ and β in the case of age-limited, cooling-limited and escape-limited acceleration, respectively. The formula $a = 2\beta$ in the age-limited case has been based on numerical simulation (Kato & Takahara, 2003; Kang et al., 2009), while the others are obtained analytically on the assumption of stationary state, and they are not yet confirmed numerically. In this paper, we study the cutoff shape of the electron spectrum by numerically solving the transport equation describing diffusive shock acceleration, and study whether the above relations are right or not.

We use a numerical method for solving cosmic-ray transport equation (so-called, diffusion-convection equation), which was proposed by Achterberg & Krüls (1992). This method is based on the equivalence between the Fokker-Planck equation and the Itô stochastic differential equation (SDE) (Gardiner, 1983). Subsequent studies have followed for various situations (Krüls & Achterberg, 1994; Yoshida & Yanagita, 1994; Marcowith & Kirk, 1999; Marcowith & 2010; Schure et al., 2010). It should be noted that the SDE method has an advantage if the transport equation has to be solved in multi-dimensions. In practice, the importance of upstream inhomogeneity for understanding of cosmic-ray acceleration at supernova remnants has been pointed out by various authors (e.g., Inoue et al., 2012). In this case, it is clear to consider the particle acceleration in three dimensions.

The simple-minded application of the SDE method has problems in actual numerical integration. First, δ -functions

appear in SDE if we apply it to the shock front, where the background fluid velocity as well as the diffusion coefficient have a sudden jump. In order to avoid this, the shock structure is artificially smoothed (Achterberg & Krüls, 1992). However, even in this case, the time step has to be small enough for the simulated particles not to miss the sharp gradient at the shock front, which significantly slows down the simulation. Furthermore, in actual simulation time, approximation of the smooth shock transition causes incorrect particle spectrum. This difficulty was solved by Zhang (2000) who used the skew Brownian motion (Harrison & Shepp, 1981) which can be solved by a scaling method that eliminated the δ -functions in the SDE. Other numerical schemes to resolve this problem have also been proposed (Marcowith & Kirk, 1999; Achterberg & Schure, 2011). Second problem is that a large dynamic range in particle momentum causes low statistical accuracy at large momenta. This difficulty was also resolved by employing a particle splitting technique (Yoshida & Yanagita, 1994).

In this paper, we first attempt to perform simulations of electron acceleration incorporating *both* methods of Zhang (2000) and particle splitting. Owing to newly developed code, simulated spectra have cutoff shape accurate enough to be compared with analytical formulae. As a first step, we focus on the cases of one-dimensional plane shock. Extended studies for more complicated cases such as time dependent free escape boundary, nonuniform magnetic fields, and/or multi-dimensional systems (including spherical shock geometry) are simple but remained as future works.

2. Basic Equations and Numerical Method

2.1. Basic equations

In this paper, we consider one-dimensional system, that is, all quantities depend on the spatial coordinate x . The diffusion-convection equation with energy-loss process is given by

$$\frac{\partial f}{\partial t} + \frac{\partial}{\partial x} \left(v f - K \frac{\partial f}{\partial x} \right) + \frac{1}{p^2} \frac{\partial}{\partial p} \left[\left(-\frac{p}{3} \frac{dv}{dx} + \frac{dp}{dt} \right) p^2 f \right] = 0 \quad , \quad (1)$$

where $f(x, p, t)$ is the distribution function for electrons, and p is the electron momentum. Functions $v(x)$ and $K(x, p)$ are background velocity field and the spatial diffusion coefficient of the electrons, respectively. In this paper, we consider the synchrotron cooling. Then, the loss term becomes

$$\frac{dp}{dt} = -\beta_{syn} \gamma p \quad , \quad (2)$$

where

$$\beta_{syn} = \frac{\sigma_T B^2}{6\pi m_e c} \quad , \quad (3)$$

and $\gamma = \sqrt{(p/m_e c)^2 + 1}$ is the electrons' Lorentz factor, and B is the magnetic field. Physical constants, σ_T , m_e

and c are Thomson cross section, mass of electron and velocity of light, respectively.

Introducing new quantities,

$$u = \ln \left(\frac{p}{m_e c} \right) \quad , \quad (4)$$

and

$$F(x, u, t) = p^3 f(x, p, t) \quad , \quad (5)$$

equation (1) becomes the Fokker-Planck form,

$$\frac{\partial F}{\partial t} + \frac{\partial}{\partial x} \left[\left(v + \frac{\partial K}{\partial x} \right) F \right] - \frac{\partial^2}{\partial x^2} (K F) - \frac{\partial}{\partial u} \left[\left(\frac{1}{3} \frac{dv}{dx} + \beta_{syn} \gamma \right) F \right] = 0 \quad . \quad (6)$$

This equation is equivalent to the following SDEs of the Itô form:

$$dx = \left(v + \frac{\partial K}{\partial x} \right) dt + \sqrt{2K} dW \quad , \quad (7)$$

$$du = - \left(\frac{1}{3} \frac{dv}{dx} + \beta_{syn} \gamma \right) dt \quad , \quad (8)$$

where dW is a Wiener process given by the Gaussian distribution:

$$P(dW) = \frac{1}{\sqrt{2\pi dt}} \exp(-dW^2/2dt) \quad . \quad (9)$$

Numerical simulation by SDEs is much faster than that with the usual Monte Carlo method and is much easier than solving the original Fokker-Planck equation, because the SDEs are ordinary differential equations.

2.2. Method of Zhang (2000)

The application of the SDEs, equations (7) and (8), for the study of electron acceleration at the shock is not simple, because the velocity field $v(x)$ has a sudden jump at the shock front, so that dv/dx in equation (8) contains δ -function. Similarly, if the diffusion coefficient also behaves discontinuously at the shock front, then $\partial K/\partial x$ in equation (7) also contains the δ -function. We take the co-moving frame with the shock which is located at $x = 0$ and we define $x < 0$ as upstream region. Following Zhang (2000), we decompose the velocity field v and the diffusion coefficient K into two parts:

$$v(x) = v_c(x) + \frac{\Delta V}{2} \text{sign}(x) \quad , \quad (10)$$

$$K(x) = K_c(x) + \frac{\Delta K}{2} \text{sign}(x) \quad , \quad (11)$$

where $\Delta V = v(0^+) - v(0^-)$ and $\Delta K = K(0^+) - K(0^-)$, and $\text{sign}(x)$ is the sign of x . Functions $v_c(x)$ and $K_c(x)$ are continuous for arbitrary x (including $x = 0$). We scale

the x coordinate according to its sign in the following way (Harrison & Shepp, 1981):

$$y = xs(x) = x \times \begin{cases} \alpha & (x < 0) \\ \frac{1}{2} & (x = 0) \\ 1 - \alpha & (x > 0) \end{cases}, \quad (12)$$

where

$$\alpha = \frac{K(0^+)}{K(0^+) + K(0^-)}. \quad (13)$$

Then, SDEs (7) and (8) can be rewritten as

$$dy = s(x) \left[\left(v(x) + \frac{\partial K_c}{\partial x} \right) dt + \sqrt{2K} dW \right], \quad (14)$$

$$du = - \left(\frac{1}{3} \frac{dv_c}{dx} + \beta_{syn} \gamma \right) dt - \frac{\Delta V}{3\Delta K} [dx - s^{-1}(y)dy]. \quad (15)$$

Derivation of equations (14) and (15) are the same way as of Zhang (2000). These equations do not contain δ -functions and can be integrated directly. Once $y(t)$ is obtained, the position of electrons $x(t)$ can be obtained by

$$x = ys^{-1}(y) = y \times \begin{cases} 1/\alpha & (y < 0) \\ 2 & (y = 0) \\ 1/(1 - \alpha) & (y > 0) \end{cases}. \quad (16)$$

In order to see the effect of diffusion, the spatial step size of diffusion in one time step Δt must be larger than that of convection, that is $v\Delta t < \sqrt{2K}\Delta t$. Hence we derive the requirement of the time step as

$$\Delta t < \frac{2K}{v^2}. \quad (17)$$

Functions $x(t)$ and $u(t)$ are numerically integrated as follows. We define $X_i = X(t_i)$ and $X_{i+1} = X(t_i + \Delta t)$, where $X = x, y$ and u . First, we discretize equation (14) as

$$y_{i+1} = y_i(x_i) + s(x_i) \left[\left(v(x_i) + \frac{\partial K_c}{\partial x}(x_i, u_i) \right) \Delta t + \sqrt{2K(x_i, u_i)} \Delta W \right], \quad (18)$$

where ΔW is independent and identically distributed normal random variable with expected value zero and variance Δt . Then, y_{i+1} is obtained for given x_i and u_i . Second, we get x_{i+1} from equation (16). Finally, u_{i+1} is calculated from equation (15), which is discretized as

$$u_{i+1} = u_i - \left(\frac{1}{3} \frac{dv_c}{dx}(x_i) + \beta_{syn} \gamma(u_i) \right) \Delta t + \Delta L, \quad (19)$$

where

$$\begin{aligned} \Delta L &= -\frac{\Delta V}{3\Delta K} [(x_{i+1} - x_i) - s^{-1}(y_i)(y_{i+1} - y_i)] \\ &= -\frac{\Delta V}{3\Delta K} [x_{i+1} - s^{-1}(y_i)y_{i+1}] \\ &= \frac{-\Delta V}{3[K(0^+) + K(0^-)]} \end{aligned}$$

$$\times \begin{cases} 0 & (x_i x_{i+1} > 0) \\ x_{i+1}/(\alpha - 1) & (x_i > 0, x_{i+1} < 0) \\ x_{i+1}/\alpha & (x_i < 0, x_{i+1} > 0) \\ |x_{i+1}| & (x_i = 0, x_{i+1} \neq 0) \\ 0 & (x_{i+1} = 0) \end{cases} \quad (20)$$

Here we use the fact $0 < \alpha < 1$ and equations (12) and (16). Now the meaning of ΔL becomes clear. Since $\Delta V < 0$ in our case (see section 3.1), one can find $\Delta L > 0$ when $x_i x_{i+1} < 0$, and $\Delta L = 0$ when $x_i x_{i+1} > 0$. Therefore, it is confirmed that particles gain energy when they pass through the shock front (Zhang, 2000).

2.3. Particle Splitting

A particle splitting is necessary to achieve a wide momentum range of accelerated electrons. Following Yoshida & Yanagisawa (1994), we set splitting surfaces u_n in momentum space ($u_{s0} < u < u_{s1}$) with an equal spacing in logarithmic scale:

$$u_n = u_{s0} + n\Delta u, \quad (21)$$

where $n = 0, 1, 2, \dots, n_{\max}$ and $\Delta u = (u_{s1} - u_{s0})/n_{\max}$. Each time an accelerated particle hits the surface u_n , the particle is split into w particles with the same energy and spatial position which particles have attained. The statistical weight which is needed to calculate the final spectrum of the particles is decreased by a factor of w in each splitting.

3. Simulations for stationary shock cases

3.1. Simulation setup

In the following, we consider electron acceleration at stationary plane parallel shock, that is,

$$v_c(x) = \frac{v_1 + v_2}{2}, \quad (22)$$

and $\Delta V = v_2 - v_1$, so that

$$v(x) = \begin{cases} v_1 & (x < 0) \\ v_2 & (x > 0) \end{cases}, \quad (23)$$

where constants v_1 and v_2 are upstream and downstream velocities, respectively. Compression ratio $r = v_1/v_2$ is fixed to be 4 throughout the paper. We also assume that the diffusion coefficient is uniform both in upstream and downstream regions, that is,

$$K_c(x) = \frac{K_1 + K_2}{2}, \quad (24)$$

and $\Delta K = K_2 - K_1$, so that

$$K(x) = \begin{cases} K_1 & (x < 0) \\ K_2 & (x > 0) \end{cases}, \quad (25)$$

where upstream and downstream coefficients, K_1 and K_2 , depend on electron momentum. In this paper, we assume

$$\begin{aligned} K_1(p) &= rK_2(p) \\ &= 1.6 \times 10^{19} B_{\mu G}^{-1} \left(\frac{p}{m_{ec}} \right)^\beta \text{ cm}^2 \text{ s}^{-1}, \quad (26) \end{aligned}$$

where $B_{\mu G}$ is the magnetic field strength in units of μG .

We set a free escape boundary at $x = -x_{\text{feb}} (< 0)$ in the upstream region. Once a particle goes beyond the boundary, it never comes back to the acceleration site. This fact becomes significant when the particle's penetration depth in the upstream region, $K_1(p)/v_1$, is comparable to x_{feb} . On the other hand, when x_{feb} is sufficiently large (i.e., $x_{\text{feb}} \rightarrow \infty$), the particle escape does not occur.

The start and end times of electron acceleration are $t = 0$ and t_{age} , respectively. During this period, electrons are injected with a momentum p_{inj} at the shock front $x = 0$ continuously at a constant rate. Taking an ensemble average over a number of realizations of SDEs, (14), (15) and (16), we obtain the momentum spectrum of the whole region (including both upstream and downstream regions as well as the shock front) at $t = t_{\text{age}}$. In the following, we consider the case $\beta > 0$. Then, $K(p)$ increases with p . Hence, if the injection momentum p_{inj} is taken so as to $\Delta t < 2K(p_{\text{inj}})/v_1^2$, the condition for time step, equation (17), is always satisfied. It can be seen from Table 2 that p_{inj} satisfies this requirement.

We perform simulations for various parameter sets. Adopted parameters are summarized in Tables 1 and 2. The cutoff shape of electron spectrum depends on how the maximum momentum of electrons is determined. In the next section, we consider three cases, age-limited, cooling-limited, and escape-limited cases, in order to decide the maximum attainable electron momentum due to the diffusive shock acceleration.

3.2. Estimate of Maximum electron momentum

The maximum momentum of accelerated electrons is limited by a finite shock age, their cooling or escape (e.g., Yamazaki et al., 2006; Ohira et al., 2012). It is obtained by comparisons of timescales, which are given as functions of electron momentum and the shock age, t_{age} in the age-limited and cooling-limited cases. The acceleration time of the diffusive shock acceleration is represented by (Drury, 1983)

$$t_{\text{acc}} = \frac{3}{v_1 - v_2} \left(\frac{K_1}{v_1} + \frac{K_2}{v_2} \right) . \quad (27)$$

Using $v_2 = v_1/r$ and equation (26) with $r = 4$, we obtain

$$t_{\text{acc}} = 1.28 \times 10^4 B_{\mu G}^{-1} v_8^{-2} \left(\frac{p}{m_e c} \right)^\beta \text{ s}^{-1} , \quad (28)$$

where v_8 is the shock velocity, v_1 , in units of 10^8 cm s^{-1} . From the condition $t_{\text{acc}} = t_{\text{age}}$, the age-limited maximum momentum, $p_{\text{m,age}}$, is derived as

$$p_{\text{m,age}} = (2.46 \times 10^5 B_{\mu G} v_8^2 t_{100})^{\frac{1}{\beta}} m_e c , \quad (29)$$

where $t_{100} = t_{\text{age}}/100 \text{ yr}$.

When the magnetic field is strong, the electron acceleration is limited by synchrotron cooling. We obtain the cooling-limited maximum momentum from the condition

$t_{\text{acc}} = t_{\text{cool}}$, where t_{cool} is the synchrotron cooling time given by

$$t_{\text{cool}} = \beta_{\text{syn}}^{-1} \left(\frac{p}{m_e c} \right)^{-1} . \quad (30)$$

Using equations (28) and (30), we derive

$$p_{\text{m,cool}} = (6.05 \times 10^{16} B_{\mu G}^{-1} v_8^2)^{\frac{1}{\beta+1}} m_e c . \quad (31)$$

It may happen that the maximum energy is limited by the escape process (Ohira et al., 2010). Characteristic spatial length of particles penetrating into the upstream region is given by $K_1(p)/v_1$. As long as $K_1(p)/v_1 \ll x_{\text{feb}}$, the particles are confined without the significant escape loss, and they are accelerated to higher energies. On the other hand, when their momentum increases up to sufficiently high energies satisfying $K_1(p)/v_1 > x_{\text{feb}}$, their acceleration ceases and they escape into the far upstream. Therefore, the maximum momentum of accelerated particles in this scenario is given by the condition

$$\frac{K_1(p)}{v_1} = x_{\text{feb}} . \quad (32)$$

This reads

$$p_{\text{m,esc}} = (6.25 \times 10^3 B_{\mu G} v_8 x_{15})^{\frac{1}{\beta}} m_e c , \quad (33)$$

where $x_{15} = x_{\text{feb}}/10^{15} \text{ cm}$.

When $p_{\text{m,age}}$ is smallest among $p_{\text{m,age}}$, $p_{\text{m,cool}}$ and $p_{\text{m,esc}}$, the acceleration is limited by the age of the shock. In the cooling-limited and escape-limited cases, $p_{\text{m,cool}}$ and $p_{\text{m,esc}}$ are smallest, respectively.

3.3. Results

Figures 1, 2 and 3 show results of numerical simulation for the age-limited, cooling-limited and escape-limited cases, respectively. The spectra in these figures are for all particles which are still in the system at t_{age} , that is,

$$F(p) \propto p^3 f(p) \propto \int_{-x_{\text{feb}}}^{\infty} F(x, u, t_{\text{age}}) dx . \quad (34)$$

The value F of the distribution function for given momentum range $[u, u + \Delta u]$ is derived by an ensemble average. If injected particles with momentum p_{inj} have a statistical weight of unity, then, particles which have experienced splitting n times have the statistical weight w^{-n} . Hence, we obtain

$$F = \sum_{\text{particles}} w^{-n} , \quad (35)$$

where summation is taken for all (split) particles which have a momentum between u and $u + \Delta u$. Error bars in spectra of figures 1–3 are calculated assuming Poisson statistics. Taking into account the propagation of errors, the statistical error ΔF for given momentum range $[u, u + \Delta u]$ is calculated as

$$(\Delta F)^2 = \sum_{\text{particles}} w^{-2n} . \quad (36)$$

Table 1: Adopted parameters in the present study.

Run ^a	β	B [μG]	v_1 [10^8cm s^{-1}]	t_{age} [yr]	x_{feb} [10^{15}cm]	p_{inj} [$m_e c$]	$p_{\text{m,age}}^b$ [$m_e c$]	$p_{\text{m,cool}}^c$ [$m_e c$]	$p_{\text{m,esc}}^d$ [$m_e c$]
A07-1	0.7	1	1	3	∞	10^3	3.4×10^5	7.4×10^9	∞
A07-2	0.7	1	1	10	∞	10^3	1.9×10^6	7.4×10^9	∞
A07-3	0.7	1	1	30	∞	10^3	9.0×10^6	7.4×10^9	∞
A07-4	0.7	1	1	100	∞	10^3	5.0×10^7	7.4×10^9	∞
A07-5	0.7	1	1	300	∞	10^3	2.4×10^8	7.4×10^9	∞
A10-1	1.0	1	6	3	∞	10^3	2.7×10^5	1.5×10^9	∞
A10-2	1.0	1	6	10	∞	10^3	8.9×10^5	1.5×10^9	∞
A10-3	1.0	1	6	30	∞	10^3	2.7×10^6	1.5×10^9	∞
A10-4	1.0	1	6	100	∞	10^3	8.9×10^6	1.5×10^9	∞
A10-5	1.0	1	6	300	∞	10^3	2.7×10^7	1.5×10^9	∞
A15-1	1.5	5	8	3	∞	10^3	1.8×10^4	1.4×10^7	∞
A15-2	1.5	5	8	10	∞	10^3	4.0×10^4	1.4×10^7	∞
A15-3	1.5	5	8	30	∞	10^3	8.2×10^4	1.4×10^7	∞
A15-4	1.5	5	8	100	∞	10^3	1.8×10^5	1.4×10^7	∞
A15-5	1.5	5	8	300	∞	10^3	3.8×10^5	1.4×10^7	∞
C07-1	0.7	2000	0.1	10	∞	10^4	1.4×10^8	5.7×10^6	∞
C07-2	0.7	500	0.1	100	∞	10^4	5.0×10^8	1.3×10^7	∞
C10-1	1.0	2000	1	10	∞	10^4	4.9×10^7	5.5×10^6	∞
C10-2	1.0	500	1	100	∞	10^4	1.2×10^8	1.1×10^7	∞
C15-1	1.5	2000	10	100	∞	10^4	1.3×10^7	1.6×10^6	∞
C15-2	1.5	500	10	800	∞	10^4	2.1×10^7	2.7×10^6	∞
E07-1	0.7	1	6	95	0.1	10^2	7.8×10^9	6.1×10^{10}	1.3×10^5
E07-2	0.7	1	6	95	1	10^2	7.8×10^9	6.1×10^{10}	3.4×10^6
E07-3	0.7	1	6	95	10	10^2	7.8×10^9	6.1×10^{10}	9.2×10^7
E07-4	0.7	1	6	95	100	10^2	7.8×10^9	6.1×10^{10}	2.5×10^9
E10-1	1.0	1	6	95	0.1	10^2	8.4×10^6	1.5×10^9	3.8×10^3
E10-2	1.0	1	6	95	1	10^2	8.4×10^6	1.5×10^9	3.8×10^4
E10-3	1.0	1	6	95	10	10^2	8.4×10^6	1.5×10^9	3.8×10^5
E10-4	1.0	1	6	95	100	10^2	8.4×10^6	1.5×10^9	3.8×10^6
E15-1	1.5	1	6	95	0.1	10^2	4.1×10^4	2.2×10^7	2.4×10^2
E15-2	1.5	1	6	95	1	10^2	4.1×10^4	2.2×10^7	1.1×10^3
E15-3	1.5	1	6	95	10	10^2	4.1×10^4	2.2×10^7	5.2×10^3
E15-4	1.5	1	6	95	100	10^2	4.1×10^4	2.2×10^7	2.4×10^4

^aA, C and E stand for age, cooling and escape, respectively.^bcalculated according to equation (29).^ccalculated according to equation (31).^dcalculated according to equation (33).

We adopt different values of u_{s1} , n_{\max} and w for different runs so as to obtain good statistics near the maximum momentum (see Appendix). Therefore, for different runs, the length of error bars is different from each other. For each case, the dependence of the cutoff shape of the electron spectrum on β is discussed below.

3.3.1. Age-limited case: $p_{m,age} < \min\{p_{m,cool}, p_{m,esc}\}$

For each value of β (0.7, 1.0 and 1.5), we had five runs with different t_{age} . One can see from figure 1 that at lower electron momentum where $p \ll p_{m,age}$, the spectrum is well described by the analytical solution in the steady state, $F(p) = p^3 f(p) \propto p^{-1}$. Furthermore, estimated values of $p_{m,age}$ (see Table 1) using equation (29) agree with the simulation result. Hence our present numerical scheme works well.

For all runs of age-limited acceleration, we have fitted the spectrum by the following function

$$F(p) \propto p^{-1} \exp \left[- \left(\frac{p}{p_m} \right)^a \right], \quad (37)$$

and obtain the value of cutoff shape parameter a . The left panel of figure 4 shows the result. One can roughly confirm earlier result of numerical simulations, $a \approx 2\beta$ (Kato & Takahara, 2003; Kang et al., 2009).

3.3.2. Cooling-limited case: $p_{m,cool} < \min\{p_{m,age}, p_{m,esc}\}$

For each value of β (0.7, 1.0 and 1.5), we performed two simulations with the magnetic field strength of $B = 2$ mG and 0.5 mG. Since the magnetic field strength B is much larger than any other cases, the requirement for time step, equation (17), is the most severe, so that we set larger p_{inj} of $10^4 m_{ec}$ in order to save the computation time.

In all runs, one can identify the cooling break, at which the spectral slope changes from p^{-1} to p^{-2} . The break energy p_b is determined by the condition $t_{cool} \approx t_{age}$ (Longair, 2011), and we derive

$$p_b \approx 2.45 \times 10^{11} B_{\mu G}^{-2} t_{100}^{-1} m_{ec}. \quad (38)$$

For example, we obtain from this equation $p_b = 6.1 \times 10^5 m_{ec}$ for run C07-1, which is consistent with the simulation result. In some runs such as C15-1 and C15-2, we can see pile-ups at the high-energy end (see the right panel of figure 2). Based on these facts, we fit spectra which were derived from simulations by the following function

$$F(p) \propto p^{-1} C_b(p) C_p(p) \exp \left[- \left(\frac{p}{p_m} \right)^a \right], \quad (39)$$

where

$$C_b(p) = \left[1 + \left(\frac{p}{p_b} \right)^w \right]^{-1/w}, \quad (40)$$

and

$$C_p(p) = \left[1 + \left(\frac{p}{\eta p_m} \right)^q \right]^{k/q}, \quad (41)$$

describe the cooling break and the pile-up effect, respectively. Middle panel of figure 4 shows the fitted a as a function of β . The result is roughly consistent with the analytical result, $a = \beta + 1$, which is derived on the steady state assumption (Zirakashvili & Aharonian, 2007; Yamazaki et al., 2013). In the case of $\beta = 1.5$, fitted value of a deviates from the analytical expectation of 2.5. This comes from the appearance of pile-up, which deforms the spectrum around the maximum momentum. Hence, it is implied that the analytical expectation $a = \beta + 1$ is not always hold when the electron pile-up becomes significant.

Previously, based on similar numerical simulation to ours, Marcowith & Casse (2010) numerically obtain the shock front energy spectra, $F_0(p) = F(x=0, p)$, for the cases of $\beta = 0, 1/2$ and 1, and confirmed the relation $a = \beta + 1$ (for smaller dynamic range of momentum than ours). In the present study, we find that at least $\beta < 1$, the relation $a = \beta + 1$ roughly holds even for the spectrum of the whole region.

3.3.3. Escape-limited case: $p_{m,esc} < \min\{p_{m,age}, p_{m,cool}\}$

In this case, steady-state spectrum at the shock front ($x = 0$) has been analytically derived as (Caprioli et al., 2009b; Reville et al., 2009; Yamazaki et al., 2013)

$$F_0(p) = F(x=0, p) \propto p^3 \exp \left[- \frac{4}{\beta} \int^{y(p)} \frac{d \log y}{1 - e^{-1/y}} \right], \quad (42)$$

where $y(p) = (p/p_m)^\beta$. For each value of β (0.7, 1.0 and 1.5), we have four runs with different x_{feb} . Then, we find that in all runs, the derived spectra are well fitted with models described by equation (42) (see figure 3). Hence, equation (42) well reproduces the spectrum of the whole region with good accuracy although it has been derived as the shock front spectrum at $x = 0$.

Here we discuss on whether the simulated spectra are fitted with phenomenological formula, equation (37). In the limit $p \gg p_m$, we can approximate $1 - e^{-1/y} \approx 1/y$ in equation (42), resulting in $F_0(p) \propto \exp[-(p/p_m)^\beta]$, so that one might expect $a = \beta$ (Yamazaki et al., 2013). If we fit numerically derived spectra with equation (37), then the fitted values of a are not along with the expectation $a = \beta$. Difference between equations (42) and (37) with $a = \beta$ is large at $p \sim p_m$. However, they seem to lie on $a \approx \beta + 0.5$ (see the right panel of figure 4). This implies that $F(p) \propto p^{-1} \exp[-(p/p_m)^\beta]$ is not a good approximation around the maximum momentum p_m .

4. Summary and Discussion

We have developed a numerical method of SDE to simulate electron acceleration at astrophysical shocks. Our code involves Zhang's method of skew Brownian motion and particle splitting. Using this code, we have performed simulations of electron acceleration at stationary plane

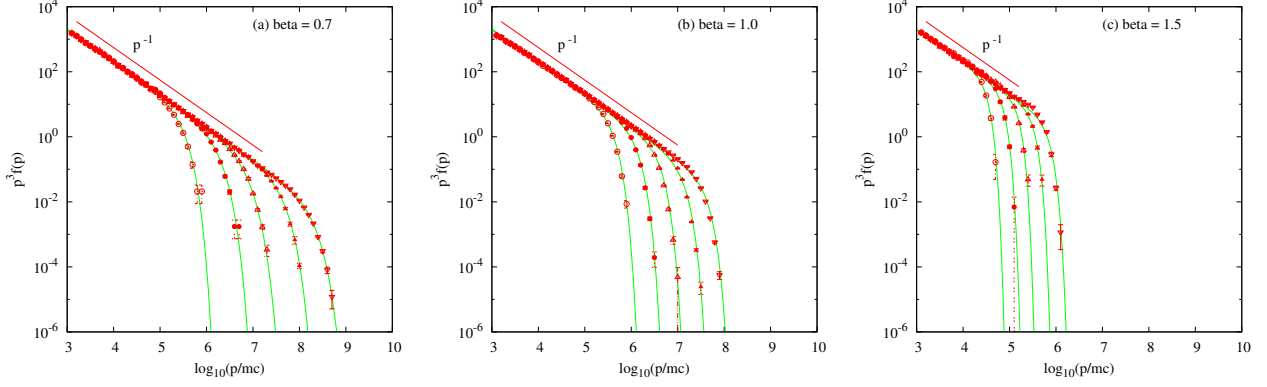


Figure 1: Electron spectra in the age-limited cases with (a) $\beta = 0.7$ (Runs A07-1, A07-2, A07-3, A07-4, A07-5 from left to right), (b) $\beta = 1.0$ (Runs A10-1, A10-2, A10-3, A10-4, A10-5 from left to right) and (c) $\beta = 1.5$ (Runs A15-1, A15-2, A15-3, A15-4, A15-5 from left to right). Lines indicate the best fitted models described by equation (37).

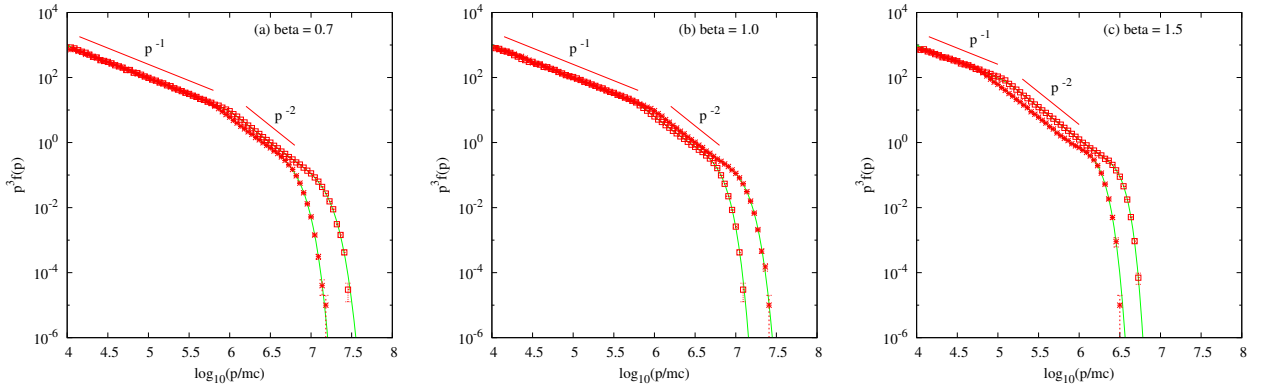


Figure 2: Electron spectra in the cooling-limited cases with (a) $\beta = 0.7$ (Runs C07-1, C07-2 from left to right), (b) $\beta = 1.0$ (Runs C10-1, C10-2 from left to right) and (c) $\beta = 1.5$ (Runs C15-1, C15-2 from left to right). Lines indicate the best fitted models described by equations (39), (40) and (41).

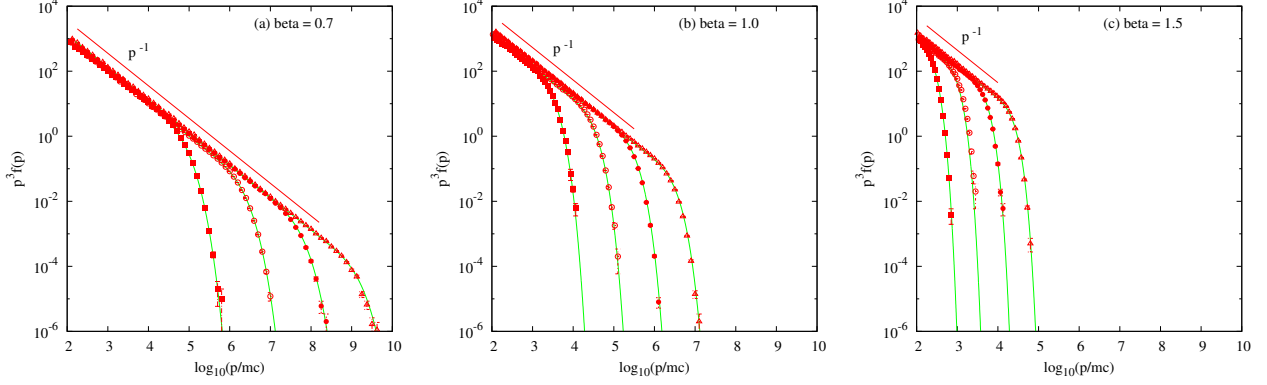


Figure 3: Electron spectra in the escape-limited cases with (a) $\beta = 0.7$ (Runs E07-1, E07-2, E07-3, E07-4 from left to right), (b) $\beta = 1.0$ (Runs E10-1, E10-2, E10-3, E10-4 from left to right) and (c) $\beta = 1.5$ (Runs E15-1, E15-2, E15-3, E15-4 from left to right). Lines indicate the best fitted models described by equation (42).

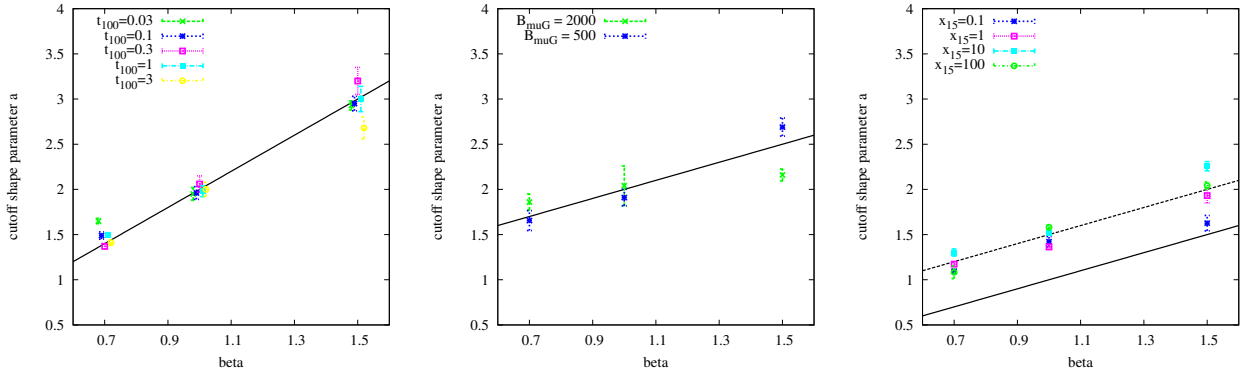


Figure 4: Cutoff shape parameter a as a function of β in the age-limited (left), cooling-limited (center) and escape-limited (right) cases. The values of a are derived by fitting the simulated spectra with the model described by equations (37) and (39) for age-limited and cooling-limited cases, respectively. Note that for escape-limited cases, we use phenomenological formula, equation (37), to derive values of a , while we used in Figure 3 the analytical stationary solution, equation (42), to fit the simulated spectra. In the left panel, data points are artificially shifted a little in the horizontal direction in order to be separated with each other and to be seen clearly. Solid lines represent $a = 2\beta$, $a = \beta + 1$ and $a = \beta$ for the age-limited, cooling-limited and escape-limited cases, respectively. The dashed line in the right panel shows $a = \beta + 0.5$.

parallel shock, and we reproduced the analytical result in the momentum range much smaller than the maximum momentum — $f(p) \propto p^{-4}$ in the age-limited and escape-limited cases, and the broken power-law which changes from $f(p) \propto p^{-4}$ to p^{-5} at the cooling break in the cooling-limited cases. These results can be achieved due to incorporation of Zhang’s method. Furthermore, the maximum electron momentum in the simulated spectra can be well explained by simple analytical argument, which is the outcome of the particle splitting method. Therefore, we believe our numerical code works well, and it enables us to study the cutoff shape of the electron spectrum.

We have performed simulations for various parameter sets, and studied how the cutoff shape, which is characterized by cutoff shape parameter a , changes with the momentum dependence of the diffusion coefficient β . In the age-limited cases, we have reproduced previous results of other authors, $a \approx 2\beta$. In the cooling-limited cases, the analytical expectation $a \approx \beta + 1$ is roughly reproduced although we recognize deviations to some extent (runs C15-1 and C15-2) when the pile-up effect is significant. However, we have found in the Bohm type diffusion, $K \propto p$ and $\beta = 1$, the cutoff shape parameter a is consistent with the analytical prediction $a = 2.0$ both in the age-limited and cooling-limited cases. Hence, if the effect of escape can be neglected, $a = 2$ should be canonical value. Note that in the present study, we have assumed plane shock geometry and constant electron injection. In reality, the SNR shock is nearly spherical although it has fluctuation (e.g., Inoue et al., 2012). In the spherical shock case, accelerated particles downstream of the shock experience adiabatic losses. This reduces the mean energy gain they experience at the shock, which steepens the spectral slope (e.g., Yamazaki et al., 2006; Schure et al., 2010). In addition, the exact spectral slope in a time-dependent calculation depends on the injection history, which may be complicated depending on the shock velocity, ambient density and so on. These effects may influence the electron spectrum. However, we are currently interested in the energy region near the upper end of the spectrum. At the given epoch, the spectrum around the maximum energy is dominated by those which are being accelerated at that time because previously accelerated particles have suffered the adiabatic losses during transported downstream of the shock. Hence, one can expect that the cutoff shape of the spectrum does not so much depend on the past acceleration history (Yamazaki et al., 2006, 2013). This issue has not yet been studied in detail except for a few works in which the spherical and planar shock cases were compared (Schure et al., 2010; Kang, 2015), and should be investigated more in future works.

The maximum momentum is sometimes determined by the escape of accelerated particles upstream. In this case, we should use the functional form given by equation (42), otherwise we should use (37) with $a = \beta + 0.5$. Electron acceleration at SNRs is sometimes limited by the escape (see figure 1 and 2 of Ohira et al., 2012), as well as proton

acceleration, which might be inferred by recent gamma-ray observation (e.g., Ohira et al., 2010). In the present study we adopt weak magnetic field in all runs of the escape-limited cases, so that synchrotron cooling effect can be neglected. Hence, our result for the escape-limited cases is applicable to the proton acceleration. The cutoff shape around the maximum proton momentum may be studied by the precise gamma-ray spectrum which will be taken in the near future.

In the present study, we have used the test particle approximation, neglecting feedback of the accelerated particles on to the plasma forming background shock structure. Not electrons but protons deform the background plasma, because they are coupled with each other through the waves excited by accelerated protons themselves. Various authors focus on the feedback processes of accelerated particles on to the magnetohydrodynamic properties around the shock. (e.g., Berezhko & Ellison, 1999; Malkov & Drury, 2001; Kang & Jones, 2005; Vladimirov et al., 2006; Terasawa et al., 2007; Caprioli et al., 2009a; Yamazaki et al., 2009; Zirakashvili & Ptuskin, 2012; Bykov et al., 2014). In such cosmic-ray modified shocks, electron acceleration is also affected by the shock deformation, and the results may be different from those in the test particle limit. These studies are remained as a future work.

Acknowledgments

Some numerical computations in this work were carried out at the Yukawa Institute Computer Facility. The authors wish to thank Tsunehiko Kato, Kohta Murase, Aya Bamba, Kazunori Kohri, Toshio Terasawa, Fumio Takahara and Hajime Takami for useful comments and discussions. We also thank anonymous referee for valuable comments to improve the paper. This work was supported in part by the fund from Research Institute, Aoyama Gakuin University (R. Y.), and by grant-in-aid from the Ministry of Education, Culture, Sports, Science, and Technology (MEXT) of Japan, No. 24-8344 (Y. O.), No. 22540264 (S. Y.).

Appendix: Parameters for numerical simulation

Parameters for numerical simulation are summarized in Table 2. Time step, Δt , must satisfy the condition (17). In the present study, it is taken to be smaller than $2K_1(p_{\text{inj}})/v_1^2$.

We need four parameters, u_{s0} , u_{s1} , n_{max} and w , to carry out particle splitting. In the present study, we set $u_{s0} = \ln(p_{\text{inj}}/m_e c)$. The other parameters are taken differently for each run.

References

- Achterberg, A. & Krüßls, W. M. 1992, A&A, 265, L13
- Achterberg, A. & Schure, K. M. 2011, MNRAS, 411, 2628
- Actis, M., Agnetta, G., Aharonian, F., et al. 2011, Experimental Astronomy, 32, 193

Table 2: Adopted parameters in the present study.

Run ^a	Δt [10 ³ s]	n_{\max}	w	p_{s1} ^b [$m_e c$]
A07-1	10	6	12	10 ^{9.0}
A07-2	10	6	12	10 ^{9.0}
A07-3	10	6	12	10 ^{9.0}
A07-4	10	6	12	10 ^{9.0}
A07-5	10	6	12	10 ^{9.0}
A10-1	10	6	12	10 ^{8.0}
A10-2	10	6	12	10 ^{8.0}
A10-3	10	6	12	10 ^{8.0}
A10-4	10	6	12	10 ^{8.0}
A10-5	10	6	12	10 ^{8.0}
A15-1	1	6	12	10 ^{9.0}
A15-2	1	6	12	10 ^{9.0}
A15-3	1	6	12	10 ^{9.0}
A15-4	1	6	12	10 ^{9.0}
A15-5	1	6	12	10 ^{9.0}
C07-1	5	5	10	10 ^{6.5}
C07-2	8	5	10	10 ^{6.5}
C10-1	0.5	5	10	10 ^{6.5}
C10-2	1	5	10	10 ^{7.0}
C15-1	0.8	5	10	10 ^{6.5}
C15-2	3.2	5	10	10 ^{6.5}
E07-1	0.11	6	10	10 ^{6.0}
E07-2	0.11	6	10	10 ^{6.0}
E07-3	0.11	6	10	10 ^{7.0}
E07-4	0.11	6	10	10 ^{7.0}
E10-1	0.11	6	10	10 ^{6.0}
E10-2	0.11	6	10	10 ^{6.0}
E10-3	0.11	6	10	10 ^{6.0}
E10-4	0.11	6	10	10 ^{6.0}
E15-1	0.11	5	4	10 ^{2.5}
E15-2	0.11	6	10	10 ^{5.5}
E15-3	0.11	6	10	10 ^{5.5}
E15-4	0.11	6	10	10 ^{5.5}

^aSee Table 1.

^b $p_{s1}/m_e c = \exp[u_{s1}]$.

- Bamba, A. et al. 2003, ApJ, 589, 827
Bamba, A. et al. 2005a, ApJ, 621, 793
Bamba, A. et al. 2005b, ApJ, 632, 294
Bell, A. R. 1978, MNRAS, 182, 147
Berezhko E. G., Ellison D. C., 1999, ApJ, 526, 385
Blandford, R. D., & Ostriker, J. P. 1978, ApJ, 221, L29
Bykov, A. M. et al. 2014, ApJ, 789, 137
Caprioli, D., Blasi, P., & Amato, E. et al. 2009a, MNRAS, 396, 895
Caprioli, D., Blasi, P., & Amato, E. 2009b, MNRAS, 396, 2065
Drury, L. O'C., 1983, Rep. Prog. Phys., 46, 973
Gardiner, C. W. 1983, Handbook of Stochastic Differential Equations (Princeton: Princeton Univ. Press)
Hailey, C. J., An, H., Blaedel, K. L., et al. 2010, in Society of Photo-Optical Instrumentation Engineers (SPIE) Conference Series, 7732, 77320T
Harrison, F. A., Craig, W. W., Christensen, F. E., et al. 2013, ApJ, 770, 103
Harrison, J. M. & Shepp, L. A. 1981, Ann. Probability, 9, 309
Inoue, T., Yamazaki, R., Inutsuka, S. et al. 2012, ApJ, 744, 71
Kang, H. 2015, J. Korean Astron. Soc., in press (arXiv:1411.7513)
Kang, H., Jones T. W., 2005, ApJ, 620, 44
Kang, H., Ryu, D., & Jones, T. W. 2009, ApJ, 695, 1273
Kato, T. N., & Takahara, F. 2003, MNRAS, 342, 639
Krüls, W. M. & Achterberg, A. 1994, A&A, 286, 314
Krymskii, G. F. 1977, Akademiia Nauk SSSR Doklady, 234, 1306
Longair, M. S. 2011, High energy astrophysics (Cambridge: Cambridge Univ. Press), section 16.3.1, p. 540
Malkov, M. A., & O'C Drury, L. 2001, Reports on Progress in Physics, 64, 429
Marcowith, A. & Casse, F. 2010, A&A, 515, A90
Marcowith, A. & Kirk, J. G. 1999, A&A, 347, 391
Ohira, Y., Murase, K. & Yamazaki, R. 2010, A&A, 513, A17
Ohira, Y., Yamazaki, R., Kawanaka, N. et al. 2012, MNRAS, 427, 91
Reville, B., Kirk, J. G., & Duffy, P. 2009, ApJ, 694, 951
Schure, K. M. et al. 2010, MNRAS, 406, 2633
Takahashi, T., Mitsuda, K., Kelley, R., et al. 2010, in Society of Photo-Optical Instrumentation Engineers (SPIE) Conference Series, 7732, 77320Z
Terasawa, T. et al. 2007, Prog. Theor. Phys. Suppl., 169, 146
Uchiyama, Y. et al. 2007, Nat, 449, 576
Vink, J. & Laming, J. M. 2003, ApJ, 584, 758
Vladimirov A., Ellison D. C., Bykov A., 2006, ApJ, 652, 1246
Yamazaki, R. et al. 2004, A&A, 416, 595
Yamazaki, R. et al. 2006, MNRAS, 371, 1975
Yamazaki, R., Kohri, K., & Katagiri, H. 2009, A&A, 495, 9
Yamazaki, R., Ohira, Y., Bamba, A., & Sawada, M. 2013, Res. Astron. Astrophys., 14, 165 (arXiv:1301.7499)
Yoshida, T. & Yanagita, S. 1994, PTP, 92, 1217
Yoshida, T. & Yanagita, S. 1997, Proc. 2nd INTEGRAL Workshop 'The Transparent Universe', ESA SP-382, 85
Zhang, M. 2000, ApJ, 541, 428
Zirakashvili, V. N., & Aharonian, F. 2007, A&A, 465, 695
Zirakashvili, V. N., & Ptuskin, V. S. 2012, Astropart. Phys., 39, 12